

# Brightening of spin- and momentum-dark excitons in transition metal dichalcogenides

Maja Feierabend, Samuel Brem, August Ekman, and Ermin Malic  
Chalmers University of Technology, Department of Physics, 412 96 Gothenburg, Sweden

Monolayer transition metal dichalcogenides (TMDs) have been in focus of current research, among others due to their remarkable exciton landscape consisting of bright and dark excitonic states. Although dark excitons are not directly visible in optical spectra, they have a large impact on exciton dynamics and hence their understanding is crucial for potential TMD-based applications. Here, we study brightening mechanisms of dark excitons via interaction with phonons and in-plane magnetic fields. We show clear signatures of momentum- and spin-dark excitons in  $\text{WS}_2$ ,  $\text{WSe}_2$  and  $\text{MoS}_2$ , while the photoluminescence of  $\text{MoSe}_2$  is only determined by the bright exciton. In particular, we reveal the mechanism behind the brightening of states that are both spin- and momentum-dark in  $\text{MoS}_2$ . Our results are in good agreement with recent experiments and contribute to a better microscopic understanding of the exciton landscape in TMDs.

Transition metal dichalcogenides (TMDs) exhibit a number of fundamentally interesting and technologically promising properties<sup>1–3</sup>. Their electronic band structure consists of multiple minima and maxima in the valence and conduction band, which - combined with the strong Coulomb interaction - leads to a variety of exciton states, cf. Fig. 1(a)<sup>1,4,5</sup>. Intervalley excitons consisting of electrons and holes located in different valleys (K,  $\Lambda$ ,  $\Gamma$ ), are momentum-dark since photons cannot provide the required momentum necessary for an indirect recombination<sup>6</sup>. Furthermore, the spin-orbit coupling gives rise to pronounced spin-splitting in both conduction and valence bands<sup>7,8</sup> leading to spin-allowed (same spin for valence and conduction band) and spin-dark (different spin) states. While bright excitons, consisting of Coulomb-bound electrons and holes in the same valley with the same spin, can be directly activated by light and have been extensively investigated in literature<sup>2,4,5,9,10</sup>, spin- and/or momentum-dark excitons need an additional brightening mechanism to be visible in optical spectra<sup>11,12</sup>. Recently, signatures of spin-dark excitons have been observed in experiments with large aperture even in the absence of a magnetic field<sup>13</sup> and hence spin-dark excitons are rather *darkish*, since they exhibit an out of plane dipole.

Dark excitons are highly interesting for TMD research, as they can lie energetically below bright excitons<sup>14–16</sup> (Fig. 1(b)) and hence have a significant impact on non-equilibrium dynamics as well as optical response of these materials. Different mechanisms can principally brighten up dark exciton states. This includes in-plane magnetic fields, which mix the spin states making spin-dark excitons visible<sup>12,17</sup>. Phonons, disorder or molecules provide an additional center-of-mass momentum to activate momentum-dark excitons<sup>18–23</sup>. In this work, we present a microscopic approach allowing us to investigate the possibility to brighten up states that are both spin- and momentum-dark. Our work is motivated by an experimental study observing a yet unidentified low-energy peak in  $\text{MoS}_2$  monolayers in presence of an in-plane magnetic field. While brightening of spin-dark excitons in tungsten-based TMDs has been well understood<sup>24–28</sup>, only little is known about spin- and momentum-dark excitons in  $\text{MoS}_2$ . Including a magnetic field in our equation-of-motion approach, we find a field-induced mixing of spin-up and spin-down states, which activates the originally spin-dark exciton

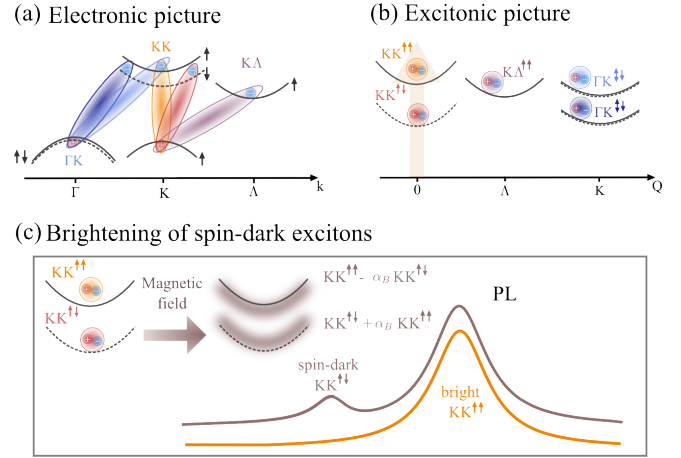


Figure 1. **Exciton dispersion and influence of a magnetic field.** (a) Electronic band structure around the high-symmetry  $\Gamma$ , K,  $\Lambda$  points including spin-orbit coupling (solid/dashed lines represent spin-up/down configurations). (b) Corresponding exciton picture with bright  $\text{KK}^{\uparrow\uparrow}$ , spin-dark  $\text{KK}^{\uparrow\downarrow}$  and momentum-dark  $\text{K}\Lambda^{\uparrow\uparrow}$ ,  $\Gamma\text{K}^{\uparrow\uparrow}$  as well as spin- and momentum-dark  $\Gamma\text{K}^{\uparrow\downarrow}$  excitons. Note that this is a schematic figure and the exact position of the corresponding valleys depend on the TMD material. (c) Brightening of spin-dark excitons due to magnetic field-induced spin-mixing of  $\text{KK}^{\uparrow\uparrow}$  and  $\text{KK}^{\uparrow\downarrow}$  states. The factor  $\alpha_B = \frac{g\mu_B B}{2\Delta}$  represents a mixing parameter that determines whether an additional peak appears in PL spectra stemming from the spin-dark exciton.

resulting in an additional peak in optical spectra, cf. Fig 1(c). Including phonon-assisted optical transitions on the same microscopic footing, we investigate the possibility to brighten up even states that are both spin- and momentum-dark.

**Theoretical approach:** To obtain a microscopic access to the optical response of TMDs after an optical excitation, we apply the density matrix formalism with semiconductor Bloch equations in its core<sup>29–32</sup>. The particular goal of this work is to describe many-particle mechanisms brightening up momentum- and spin-dark states. The intensity of photoluminescence (PL) can be expressed as<sup>22,23,33</sup>

$$I(\omega_q) \propto \hbar\omega_q \partial_t \langle c_q^\dagger c_q \rangle \propto \Im [ \langle c_q^\dagger X_q^b \rangle ]. \quad (1)$$

The PL is given by the time derivative of the photon den-

sity  $\langle c_q^\dagger c_q \rangle$  that is determined by the photon-assisted polarization  $\langle c_q^\dagger X_q^b \rangle$  corresponding to the recombination of an exciton ( $X_q^b$ ) under emission of a photon ( $c_q^\dagger$ ). Here, we have introduced the photon creation and annihilation operators  $c_q^\dagger, c_q$  and the exciton annihilation operator  $X_q^b$  that will be defined below. The introduced PL equation only describes direct radiative recombination processes and thus contains only signatures from the bright exciton. To include also possible features stemming from dark excitons via higher order processes, we have to extend the PL equation by implementing phonon-assisted radiative recombination processes and the impact of a magnetic field.

To account for excitonic effects, which are dominant in TMD monolayers<sup>2,5,9,10,34</sup>, it is convenient to project the many-particle system into an excitonic basis. Following Katsch et al.<sup>35</sup>, we introduce the exciton operator  $X_Q = \sum_q \varphi_q^* a_{q-\alpha Q} c_{q+\beta Q}^v$ , which includes the exciton wavefunction  $\varphi_q^*$  as solutions from the Wannier equation<sup>5,15,23,29,30</sup>, the electron (hole) operator  $a^{c(v)\dagger}$  and relative  $q$  and center of mass  $Q$  momenta. They can be translated into electron and hole momenta via  $q = \alpha k_e + \beta k_h$  and  $Q = k_h - k_e$  with  $\alpha(\beta) = \frac{m_e(m_h)}{m_e+m_h}$ . By introducing the exciton operator in the pair-space, we can define an excitonic Hamilton operator including the interaction with phonons and a magnetic field. The Hamiltonian reads  $H = H_0 + H_{x\text{-phot}} + H_{x\text{-phon}} + H_{x\text{-magn}}$ , where  $H_0 = \sum_{Q,i} \varepsilon_Q^i X_Q^\dagger X_Q^i + \sum_{Q,\sigma} \hbar\omega_Q^\sigma c_Q^\dagger c_Q^\sigma + \sum_{Q,\zeta} \hbar\Omega_Q^\zeta B_Q^\zeta B_Q^\zeta$  is the interaction-free part for excitons, photons and phonons with the excitonic energy  $\varepsilon_Q^i$  in the state  $i = (s_i, \eta_i)$  with the spin  $s_i = \uparrow\uparrow, \uparrow\downarrow, \downarrow\uparrow, \downarrow\downarrow$  and the valley  $\eta_i = (\text{KK}, \text{KK}', \text{K}\Lambda, \text{K}'\Lambda)$ , the photon energy  $\hbar\omega_Q^\sigma$  with the polarization mode  $\sigma$ , and the phonon energy  $\hbar\Omega_Q^\zeta$  with the phonon mode  $\zeta$ . The exciton-photon interaction reads  $H_{x\text{-phot}} = \sum_{Q,i,\sigma} M_Q^{i\sigma} c_Q^\dagger X_Q^i + \text{h.c.}$  with the optical matrix element  $M_Q^{i\sigma}$ <sup>35,36</sup>. Finally, the interaction between excitonic spin states  $i, j$  and an in-plane magnetic field  $B$  is described by the Hamiltonian

$$H_{x\text{-magn}} = \sum_{Q,i,j} G^{ij} \frac{\mu_B}{2} B X_Q^\dagger X_Q^j. \quad (2)$$

The matrix element  $G^{ij}$  reads in excitonic basis  $G^{ij} = \left( g_{ij}^c \delta_{s_i^h, s_j^h} - g_{ij}^v \delta_{s_i^e, s_j^e} \right) \sum_q \varphi_q^i \varphi_q^{j*}$  with the electrons (holes) keeping their spins, while mixing of spins in the valence (conduction) band of one valley takes place, i.e.  $g_{ij}^{c(v)} = g_{\eta_i}^{c(v)} \delta_{\eta_i, \eta_j} (1 - \delta_{s_i^e(h), s_j^e(h)})$ . Here,  $g_{\eta_i}^{c(v)}$  is the experimentally accessible g-factor for the conduction (valence) band in the valley  $\eta_i$  and  $\mu_B$  is the Bohr magneton. The g-factors in 2D materials are an ongoing topic of research<sup>37-40</sup> and still under debate as they can differ significantly for bright, dark and charged states. However, for the scope of this work, as we are interested in the qualitative behavior of dark states under magnetic fields, we assume  $g_{\eta_i}^{c(v)} \approx 4$  for all states and materials (experimental values for the bright state are  $g_{\text{MoSe}_2} = 4.2, g_{\text{WS}_2} = 4.3, g_{\text{WS}_2} = 4.0$ <sup>40</sup>).

Now, we have all ingredients at hand to derive the equation of motion for our key quantity, the photon-assisted polarization  $\langle c_q^\dagger X_q^b \rangle$  providing access to the PL, cf. Eq. (1). However, the equation can be simplified resulting in an intuitive Elliott-like formula including both phonon- and magnetic field-induced PL. To get there, we perform a unitary transformation to include the magnetic field into  $H_0$  and subsequently apply a cluster expansion approach to account for phonon-assisted radiative recombinations. We start by modifying the system with an unitary transformation, such that  $H_{x\text{-magn}}$  becomes included in  $H_0$ . To illustrate the idea, we simplify our system for now and assume an excitonic state  $i = (s_i, \eta)$  with  $Q \approx 0$  with different spins  $s_i, s_j = \uparrow\uparrow, \uparrow\downarrow$  but same valley  $\eta_i = \eta_j$ . We can decouple the appearing spin-up and spin-down states and decompose the appearing matrix element  $G^{ij}$  into a spin-subspace with Pauli matrices, and we find the field-induced mixing (neglecting for the moment the impact of photons and phonons)

$$H = \sum_{s_i, s_j} \varepsilon_{s_i}^\eta X_{s_i}^\dagger X_{s_i}^\eta + G_{s_i s_j}^\eta \frac{\mu_B}{2} B X_{s_i}^\dagger X_{s_j}^\eta = \sum_i \tilde{\varepsilon}_i^\eta \tilde{X}_i^{\eta\dagger} \tilde{X}_i^\eta$$

with the new quantum number  $i$ , new energy  $\tilde{\varepsilon}_i^\eta = \varepsilon_i^\eta \pm \sqrt{\left(\frac{\Delta^\eta}{2}\right)^2 + \left(\frac{g}{2}\mu_B B\right)^2}$ , and the new state operator  $\tilde{X}_i^{\eta(\dagger)} = U_{i1}^\eta X_{\uparrow\uparrow}^{\eta(\dagger)} + U_{i2}^\eta X_{\uparrow\downarrow}^{\eta(\dagger)} = \frac{1}{\sqrt{1+h_i^\eta}} \left( h_i^\eta X_{\uparrow\uparrow}^{\eta(\dagger)} + X_{\uparrow\downarrow}^{\eta(\dagger)} \right)$ , where we used the abbreviations  $h_i^\eta = \Delta^\eta / (g\mu_B B) + \lambda_i \sqrt{1 + \Delta^{\eta 2} / (g\mu_B B)^2}$ ,  $\Delta^\eta = \varepsilon_{\uparrow\uparrow}^\eta - \varepsilon_{\uparrow\downarrow}^\eta$  and  $\lambda_i = \pm$ . The latter can be positive or negative depending on the energetic ordering in the investigated TMD material. Note that for the definition of the transformation matrix  $\hat{U}^\eta$ , we exploited  $\tilde{X}_i^{\eta\dagger} = \hat{U}^\eta X_i^{\eta\dagger} = \sum_j U_{ij}^\eta X_j^{\eta\dagger}$  and  $\hat{U}^{\eta\dagger} \hat{U}^\eta = \mathbb{1}$ , i.e. a unitary transformation.

We can now transform the rest of the Hamilton operator into this basis, yielding for the exciton-photon coupling  $H_{x\text{-phot}} = \sum_i \tilde{M}_i c \tilde{X}_i^{\eta\dagger} + \text{h.c.}$  with the new matrix elements  $\tilde{M}_i = M U_{1i}$ . Neglecting for the moment the interaction with phonons (hence  $q \approx 0$ ), we derive the equation of motions for the photon-assisted polarization appearing in Eq. (1):

$$i\hbar\partial_t \langle c^\dagger \tilde{X}_i^\eta \rangle = (\tilde{\varepsilon}_i^\eta - \hbar\omega) \langle c^\dagger \tilde{X}_i^\eta \rangle - \tilde{M}_i^\eta \langle \tilde{X}_i^{\eta\dagger} \tilde{X}_i^\eta \rangle. \quad (3)$$

To calculate the PL intensity in presence of a magnetic field we solve this equation in the adiabatic limit<sup>23,29,30</sup> yielding

$$I(\omega) \propto \hbar\omega \Im \sum_{i\eta} \frac{(\tilde{M}_i^\eta)^2 N_i^\eta}{\tilde{\varepsilon}_i^\eta - \hbar\omega - i\gamma_i^\eta} \quad (4)$$

with the exciton occupations  $N_i^\eta$ , excitonic energy  $\tilde{\varepsilon}_i^\eta$  and dephasing  $\gamma_i^\eta$ , where  $\eta$  and  $i$  are the exciton and spin index.

**Brightening of spin-dark excitons:** For a better understanding of the influence of the magnetic field, we disregard for the moment the impact of momentum-dark excitons and consider only the bright state  $\eta = \text{KK}, i = \uparrow\uparrow$  (denoted by B) and the spin-dark state  $\eta = \text{KK}, i = \uparrow\downarrow$  (denoted by D). Furthermore we consider the situation  $\mu_B B \ll \Delta^\eta$ , where the

energy difference between spin-allowed and spin-dark state is large compared to the Zeeman splitting. Here, the Zeeman term gives only a small correction to the energy, which is the case in tungsten-based TMDs for experimentally available magnetic field strengths. Then, we split up the sum over  $\eta$  in Eq. (4) into dark and bright state and enter the solutions  $M_i^\eta = MU_{1i}^\eta$ . Moreover, we set  $U^\eta = \text{const}$  for the bright states and perform a Taylor expansion of  $U^\eta$  for the dark states. This results in a more intuitive expression for the PL

$$I \propto \hbar\omega \Im \left[ \frac{M^2 N_B}{\varepsilon_B - \hbar\omega - i\gamma_B} + \frac{M^2 \left( \frac{g\mu_B B}{2\Delta^{\text{KK}}} \right)^2 N_D}{\varepsilon_D - \hbar\omega - i\gamma_D} \right]. \quad (5)$$

The first term describes the direct PL contribution stemming from the bright  $\text{KK}^{\uparrow\uparrow}$  exciton and resulting in a resonance at the energy  $\varepsilon_B$ . In addition, the magnetic field appearing in the second term gives rise to a new resonance at the position  $\varepsilon_D$  due to the activation of spin-dark excitons. Assuming that excitons quickly thermalize, exciton densities can be approximated by equilibrium Boltzmann distributions<sup>14,23</sup>.

Now, we numerically evaluate Eq. (5) to calculate the PL spectrum of  $\text{WSe}_2$  as an exemplary TMD material. Figure 2(a) shows the PL spectrum at a temperature of 35 K with (blue) and without (orange) the magnetic field. The peak at 1.745 eV corresponds to the bright exciton, while the extremely pronounced peak at 1.69 eV stems from the brightened spin-dark exciton. The intensity of the peak is given by both the exciton occupation  $N_D$  and the magnetic field strength assuming the same dephasing rates  $\gamma_D = \gamma_B$ . We find a quadratic B-field dependence for the PL intensity ratio between the dark (D) and the bright state (B) - in good agreement with experimental observations<sup>12,17</sup>. This reflects the prefactor  $\left( \frac{g\mu_B B}{2\Delta} \right)^2$  in Eq. (5). Here, TMD specific parameters, such as the energetic difference between the dark and bright state  $\Delta$  and the g-factor, play an important role.

Figure 2(b) shows a surface plot illustrating the dependence of PL on the magnetic field. The stronger the field, the more efficient is the brightening of the spin-dark exciton and the more pronounced is its PL peak. Furthermore, for an in-plane magnetic field, the Zeeman shift is known to be negligible and therefore we do not observe a shift in energy<sup>12</sup>. The dark exciton peak starts to appear for magnetic fields  $B > 2$  T at the considered exemplary temperature of 35 K. Exploiting Eq. (5), we find an analytic expression for the intensity ratio  $I(D)/I(B) = \xi(\text{TMD}, T) B^2$  which reveals the quadratic behavior shown in the inset of Fig. 2(a). The curvature of the parabola  $\xi(\text{TMD}, T) = \frac{\mu_B}{2} \frac{\varepsilon_D}{\varepsilon_B} \frac{N_D(T)}{N_B(T)} \frac{g}{\Delta}$  is TMD-specific and depends specifically on the (i) relative energetic position of dark and bright excitons ( $\frac{\varepsilon_D}{\varepsilon_B} \approx 1$ ), (ii) the TMD-specific g-factor and dark-bright energy splitting  $\Delta$ , and (iii) the relative temperature-dependent exciton densities ( $\frac{N_D}{N_B} = e^{-\frac{(\varepsilon_D - \varepsilon_B)}{k_B T}}$ ). In materials with  $\varepsilon_D > \varepsilon_B$  (e.g.  $\text{MoSe}_2$ ) this factor will quickly approach 0 at low temperatures and hence we do not expect the dark state to brighten up, since its occupation is very low. On the other side, for tungsten-based materials with  $\varepsilon_D < \varepsilon_B$  the factor

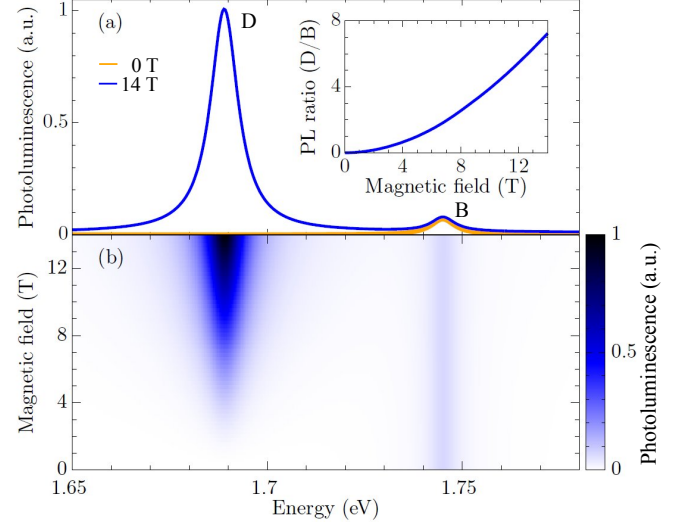


Figure 2. **Brightening of spin-dark excitons.** Photoluminescence of hBN-encapsulated  $\text{WSe}_2$  monolayer at an exemplary low temperature of 35 K with and without a magnetic field. Note that exciton-phonon scattering and phonon-sidebands have been neglected in this study. (a) While the PL at 0 T is determined by the bright  $\text{KK}^{\uparrow\uparrow}$  exciton at 1.745 eV, at 14 T the PL is clearly dominated by a new resonance at 1.69 eV stemming from the spin-dark  $\text{KK}^{\uparrow\downarrow}$  exciton. The inset reveals a quadratic behavior for the dark-bright peak ratio. (b) Surface plot of the PL as a function of energy and magnetic field strength. Note that the spectra are normalized to the bright exciton peak. The spin-dark exciton becomes visible from approximately 2 T on and grows with the magnetic field.

will instead approach infinity at low temperatures and enables pronounced brightening of dark states. However, as the temperature increases the factor  $\frac{N_D}{N_B}$  becomes smaller and hence the intensity of the peaks decreases as dark excitons thermalize and recombine via phonons. This is why spin-dark states are observed mainly at low temperatures<sup>12,17</sup>. For the curvature we can extract  $\xi(\text{WS}_2, 35 \text{ K}) = 0.0018 \text{ T}^{-2}$  and  $\xi(\text{WSe}_2, 35 \text{ K}) = 0.0038 \text{ T}^{-2}$ . This means that  $\text{WSe}_2$  is by a factor of two more responsive to an external magnetic field, which is in good agreement with experimentally observed values<sup>12</sup>. Note that slight differences in the g-factor of the two materials are expected to slightly change the difference in the curvature.

**Brightening of spin- and momentum-dark excitons:** So far, we have only included the effect of phonons in the linewidth of the exciton resonances<sup>6,23,36</sup>. However, under certain circumstances phonons can drive indirect radiative transitions from momentum-dark states<sup>19,23</sup>. Hence, to fully understand the influence of the magnetic field on PL spectra, we now include exciton-phonon scattering and consider both momentum- and spin-dark exciton states.

We extend the exciton Hamiltonian by the exciton-phonon coupling

$$H_{\text{x-phon}} = \sum_{\substack{Q, Q' \\ \eta_1, \eta_2, l, j, \zeta}} D_{Q'}^{\eta_1 l \eta_2 j \zeta} \tilde{X}_{Q+Q'}^{\dagger \eta_1 l} \tilde{X}_Q^{\eta_2 j} B_{-Q'}^{\dagger \zeta} + \text{h.c.} \quad (6)$$

which creates an exciton with the momentum  $Q + Q'$  in the state  $\eta_1, l$  and annihilates an exciton with the momentum  $Q$  in the state  $\eta_2, j$  under creation of a phonon with the momentum  $-Q'$  and the mode  $\zeta = (\text{LA, TA, LO, TO})$ . The exciton-phonon matrix element in the magnetic field basis reads  $D_{Q'}^{\eta_1 l \eta_2 j \zeta} = \sum_{k, \lambda, n, i} U_{nl}^{\eta_1} \left( \varphi_k^{\eta_1 *} d_{Q'\zeta}^\lambda \varphi_{k+\xi^\lambda Q'}^{\eta_2} \right) U_{ij}^{\eta_2 *}$  with transformation matrices  $U_{nl}^{\eta_1(\eta_2)*}$ . Here,  $d_{Q\zeta}^\lambda$  denotes the electron-phonon coupling elements in the band  $\lambda = (c, v)$ <sup>23</sup>. Furthermore, we introduced  $\xi^\lambda = \alpha, \beta$  with excitonic mass factors  $\alpha(\beta) = \frac{m_e(m_h)}{m_e + m_h}$  for the valence(conduction) band. We can see that the phonon introduces a momentum  $Q'$  into the system, which is transferred to the exciton. Depending on the efficiency of the exciton-phonon coupling, this can lead to the activation of momentum-dark excitons<sup>23</sup>.

The transformation into the magnetic field basis enables us to exploit the TMD Bloch equations for phonon-assisted photoluminescence derived in our previous work<sup>23</sup> with the modified optical matrix element  $\tilde{M}_i^\eta \rightarrow \tilde{M}^\mu$  and exciton energies  $\tilde{\varepsilon}_i^\eta + \frac{\hbar^2 Q^2}{2m\eta_i} \rightarrow \tilde{\varepsilon}_Q^\mu$  with the compound index  $\mu = \eta, i$ . We obtain a new expression for direct photoluminescence

$$I(\omega)^b \propto \sum_{\mu} \frac{|\tilde{M}^\mu|^2 \gamma_0^\mu N_0^\mu}{(\tilde{\varepsilon}_0^\mu - \omega)^2 + (\gamma_0^\mu + \Gamma_0^\mu)^2}, \quad (7)$$

which is analogue to Eq. (4) but now not only includes the radiative dephasing  $\gamma_0^\mu$  but also phonon-induced dephasing  $\Gamma_{\mathbf{Q}}^\mu$ . For the indirect phonon-assisted photoluminescence allowing us to reach momentum-dark excitons we obtain the expression

$$I(\omega)^d \propto \sum_{\mu\nu\mathbf{Q},\zeta\pm} \Omega^\mu(\omega) \frac{|\tilde{D}_{\zeta\mathbf{Q}}^{\mu\nu}|^2 N_{\mathbf{Q}}^\nu \eta_{\zeta\mathbf{Q}}^\pm \Gamma_{\mathbf{Q}}^\nu}{(\tilde{\varepsilon}_{\mathbf{Q}}^\nu \pm \Omega_{\mathbf{Q}}^\zeta - \omega)^2 + (\Gamma_{\mathbf{Q}}^\nu)^2}, \quad (8)$$

where we have introduced the abbreviation  $\Omega^\mu(\omega) = \frac{|\tilde{M}^\mu|^2}{(\tilde{\varepsilon}_0^\mu - \omega)^2 + (\gamma_0^\mu + \Gamma_0^\mu)^2}$  determining i.a. the oscillator strength. The position of the new phonon-induced signatures in the PL is determined by the energy of the exciton  $\tilde{\varepsilon}_{\mathbf{Q}}^\nu$  and the energy of the involved phonon  $\pm\Omega_{\mathbf{Q}}^\zeta$ . The sign describes either the absorption (+) or emission (-) of phonons. We take into account all in-plane optical and acoustic phonon-modes. Moreover, the appearing phonon occupation  $\eta_{\zeta\mathbf{Q}}^\pm = \left( \frac{1}{2} \mp \frac{1}{2} + n_{\zeta\mathbf{Q}}^{\text{phon}} \right)$  is assumed to correspond to the Bose equilibrium distribution according to the bath approximation<sup>41</sup>. Since dark states can not decay radiatively, the peak width is only given by non-radiative dephasing processes  $\Gamma_{\mathbf{Q}}^\nu$ . The total photoluminescence in presence of phonons and magnetic fields is obtained by adding Eq. (7) and Eq. (8), which now includes mixing of spin and momenta by the appearing sums  $\mu = \text{KK}^{\uparrow\uparrow}, \text{KK}^{\uparrow\downarrow}$  and  $\nu = \text{KK}^{\uparrow\downarrow}, \text{KK}^{\downarrow\uparrow}, \text{K}\Lambda^{\uparrow\downarrow}, \Gamma\text{K}^{\uparrow\uparrow}, \Gamma\text{K}^{\downarrow\downarrow}$ .

Now, we investigate the PL spectra at an exemplary low temperature of 35 K for both tungsten- and molybdenum-based TMDs, cf. Fig. 3. We directly compare the spectrum with and without the presence of a magnetic field. The lower panel of each picture shows the differential PL directly illustrating the impact of the field. The first observation is that even without the magnetic field additional low-energy

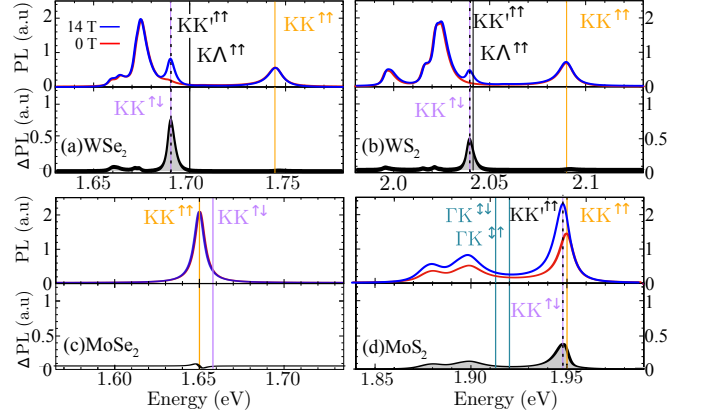


**Figure 3. Brightening of spin- and momentum-dark states.** PL with and without a magnetic field studied at 35 K for different hBN-encapsulated TMD monolayers. The lower panels show the PL difference  $\Delta\text{PL} = I_{14\text{T}} - I_{0\text{T}}$  illustrating directly the impact of the magnetic field. Without the latter, the PL in all TMDs but MoSe<sub>2</sub> is dominated by phonon-sidebands of momentum-dark  $\text{KK}^{\uparrow\uparrow}$ ,  $\text{K}\Lambda^{\uparrow\uparrow}$  or  $\Gamma\text{K}^{\uparrow\uparrow}$  excitons. They are located approx. 50-100 meV below the bright  $\text{KK}^{\uparrow\uparrow}$  state. In presence of a magnetic field, additional shoulders are observed at the position of spin-dark  $\text{KK}^{\uparrow\downarrow}$  or below the  $\Gamma\text{K}^{\uparrow\downarrow, \downarrow\uparrow}$  excitons. The latter state appearing in MoS<sub>2</sub> is both spin- and momentum-dark and requires brightening via both phonons and an in-plane magnetic field.

signatures are observed in most TMD materials. They stem from momentum-dark states (black vertical lines) and are activated via phonon-assisted radiative recombination<sup>23</sup>. In the case of WSe<sub>2</sub>, the peaks between 1.65 and 1.70 eV stem from phonon emission and absorption from energetically lower lying  $\text{KK}^{\uparrow\uparrow}$  and  $\text{K}\Lambda^{\uparrow\uparrow}$  excitons, respectively, cf. the red line in Fig. 3(a). Those phonon-sidebands appear since phonons add an additional center-of-mass momentum allowing excitons to recombine. The features are not observed directly at the position of these excitons, but are shifted by the energy of the involved phonon, i.e.  $\tilde{\varepsilon}_{\mathbf{Q}}^\nu \pm \Omega_{\mathbf{Q}}^\zeta$  (see Eq. (8)), where + is phonon absorption and - phonon emission. At low temperatures, phonon emission is dominant and hence the phonon sidebands are located 15-50 meV below the exciton position, corresponding to the phonon energies of LO/LA and TO/TA phonons. For WS<sub>2</sub>, we obtain a similar picture. The differences can be explained by different phonon energies and occupations and energetic positions of momentum-dark  $\text{KK}^{\uparrow\uparrow}$  and  $\text{K}\Lambda^{\uparrow\uparrow}$  excitons (cf. black vertical lines). Note that in principal all excitonic states exhibit phonon sidebands but only the energetically lowest one have a sufficient occupation to be visible in PL.

As MoSe<sub>2</sub> does not exhibit any energetically lower lying dark excitonic states<sup>7,15</sup>, its PL is dominated by the bright  $\text{KK}^{\uparrow\uparrow}$  exciton, cf. Fig. 3(c). For MoS<sub>2</sub>, the energetically lowest state is the momentum-dark  $\Gamma\text{K}$  which is degenerated and exhibits energetically close lying spin-allowed and spin-forbidden  $\uparrow\uparrow, \uparrow\downarrow, \downarrow\uparrow$  and  $\downarrow\downarrow$  states. This degeneracy leads, in combination with overlapping phonon replica, to broader low

energy peaks between 1.86 and 1.91 eV, cf. Fig. 3(d). Moreover, the lower energy shoulder of the bright peak can be explained by phonon replica of the  $KK^{\uparrow\uparrow}$  exciton. Note that the linewidths of the peaks are calculated on a microscopic level (for more details see our previous work<sup>6,36,42</sup>) and are in good agreement with experiments<sup>12</sup>. Since the phonon replica and linewidths are very sensitive to the exact position and contributions of the valleys<sup>42</sup>, the appearance of phonon sidebands can be a signatures of lower lying  $\Gamma K$  excitons in  $MoS_2$ .

Now, we investigate the changes of PL signatures in presence of a magnetic field, cf. blue lines in Fig. 3 and for a better illustration the differential PL spectra  $\Delta PL = I_{14T} - I_{0T}$  in the lower panels of the figure. We observe for both tungsten-based TMDs and  $MoS_2$  an upcoming peak around 50-70 meV below the bright  $KK^{\uparrow\uparrow}$ . We can trace back this new peaks to the activation of (i) spin-dark  $KK^{\uparrow\downarrow}$  excitons in  $WSe_2$  and  $WS_2$ , and (ii) spin- and momentum-dark  $\Gamma K^{\uparrow\downarrow}$  and  $\Gamma K^{\downarrow\uparrow}$  states in  $MoS_2$ . Moreover,  $MoS_2$  exhibits an additional peak just below the bright  $KK$  exciton which can be assigned to the spin-dark  $KK^{\uparrow\downarrow}$  exciton. In contrast,  $MoSe_2$  does not exhibit any additional field- or phonon-induced peaks. This reflects the excitonic landscape in this material with the bright  $KK^{\uparrow\uparrow}$  as the energetically lowest state<sup>15,16</sup>. Note that very recent experiments by Lu et al.<sup>43</sup> and Robert et al.<sup>44</sup> observed an upcoming peak 1-2 meV above the bright peak in  $MoSe_2$  in very high magnetic field ( $B \approx 30-60$  T), suggesting a possible brightening of  $KK^{\uparrow\downarrow}$  excitons in these materials. Note that we find small shifts at the position of the  $KK^{\uparrow\uparrow}$  exciton reflecting the Zeeman shift. It is in the range of  $10^{-1}$  meV and only visible in the differential PL spectra.

The field-induced difference in the PL between tungsten- and molybdenum-based TMDs stems from different underlying brightening mechanisms: While in  $WSe_2$  and  $WS_2$  the magnetic field induces a mixing of spin-allowed and spin-forbidden  $KK$  excitons, resulting in a peak at the position of the spin forbidden  $KK^{\uparrow\downarrow}$  exciton, in  $MoS_2$  it additionally couples spin-allowed and momentum-dark  $\Gamma K^{\uparrow\uparrow}$  states with spin- and momentum-dark  $\Gamma K^{\uparrow\downarrow, \downarrow\uparrow}$  excitons, resulting in phonon replica energetically below these  $\Gamma K^{\uparrow\downarrow, \downarrow\uparrow}$  states. The strong mixing of spin- and momentum-dark states in  $MoS_2$  can be traced back to the degeneracy of the states and the strong electron-phonon matrix elements<sup>45,46</sup>. Since there is no splitting of spin-states in the valence band of the  $\Gamma$  valley and since the splitting is small in the conduction band (in the range of 3 meV)<sup>7</sup>,  $\Gamma K$  excitons are energetically very close enhancing the interaction and mixing of these states. Note that the splitting in the  $\Gamma$  states is more pronounced in the excitonic picture, i.e.  $\varepsilon_{\Gamma K}^{\uparrow\uparrow} - \varepsilon_{\Gamma K}^{\uparrow\downarrow} = 8$  meV due to the influence of different exciton masses. In tungsten-based TMDs, the spin- and momentum-dark  $KK^{\uparrow\downarrow}$  and  $KA^{\uparrow\downarrow}$  states are energetically higher than the bright state<sup>7,15,16</sup> and hence do not contribute to the PL due to the very low occupation.

Comparing our results with experimental observations<sup>12</sup>, we find a very good qualitative agreement of the field-dependent PL in all four TMDs. Both theory and experiment find an additional narrow peak in tungsten-based TMDs, a broad low-energy peak in  $MoS_2$  and no field-induced signatures in  $MoSe_2$  in the investigated magnetic fields of up to

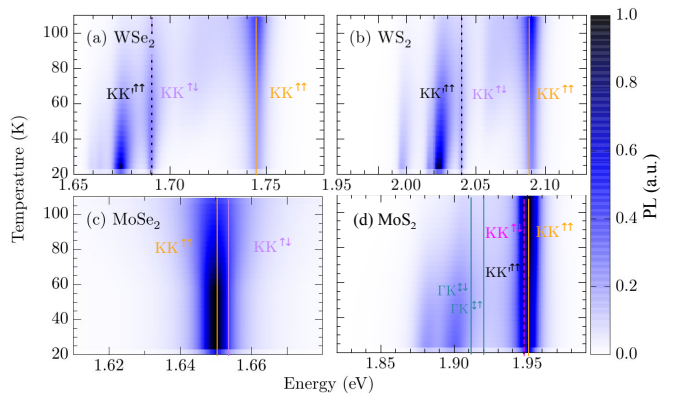


**Figure 4. Temperature dependence of PL in magnetic field.** Temperature dependence of photoluminescence in different TMD monolayers at the fixed magnetic field of 14 T. Dark exciton signatures can be observed up to 100 K in tungsten-based materials. In  $MoS_2$ , the resonances are much broader due to the overlap of phonon-sidebands of spin- and momentum-dark  $\Gamma K$  excitons.

15 T. Note that in the experiment a peak splitting of the spin-dark resonance appears in the presence of a magnetic field, which can be ascribed to the Coulomb exchange interaction<sup>12</sup> that has not been taken into account in our model. Since the exchange interaction only affects momentum-allowed states<sup>47</sup>, the splitting does not occur for  $MoS_2$ , where spin and momentum-dark  $\Gamma K^{\uparrow\downarrow}$  excitons play the crucial role.

So far we have discussed PL signatures of dark states at one exemplary temperature. Now, we vary the temperature and investigate how the impact of the magnetic field and phonons changes, cf. Fig. 4. We assume a constant magnetic field of 14 T for all investigated TMDs. We find for tungsten-based TMDs that at low temperatures, the lowest resonances stemming from  $KK^{\uparrow\uparrow}$  and  $KK^{\uparrow\downarrow}$  excitons dominate the PL spectrum, while at temperature above 60 K the bright peak becomes crucial - in agreement with experimental results<sup>24</sup>. Note that the intensity dependence on the temperature is a result of an interplay between phonon and exciton occupations in the corresponding exciton state on the one side and the exciton-phonon scattering determining the linewidth of the resonance on the other side<sup>6,23,36</sup>.

For molybdenum-based materials, we find that  $MoSe_2$  is dominated by the bright  $KK^{\uparrow\uparrow}$  exciton at all temperatures, however exhibiting an increased peak broadening at higher temperatures due to the enhanced exciton-phonon interaction. In contrast,  $MoS_2$  shows even at low temperatures two broad peaks stemming from (i) phonon sidebands of the spin- and momentum-dark  $\Gamma K^{\uparrow\downarrow, \downarrow\uparrow}$  excitons and (ii) direct emission from the momentum-allowed  $KK^{\uparrow\downarrow}$  exciton around 1.95 eV. With increasing temperature, the indirect peaks become broader and decreases in intensity due to enhanced exciton-phonon scattering.

**Conclusions:** We have investigated the impact of an in-plane magnetic field on optical properties of transition metal dichalcogenides. Exploiting a fully quantum-mechanical and

microscopic approach, we provide insights into signatures of momentum- and spin-dark excitons in photoluminescence spectra. We find that the field-induced mixing of spin-up and spin-down states results in a brightening of spin-dark excitons resulting in new resonances. We show that the origin of the new peak is the direct emission of the  $KK^{\uparrow\downarrow}$  exciton in tungsten-based materials, whereas for  $\text{MoS}_2$  it is the indirect, phonon-induced transition from the spin- and momentum-dark  $\Gamma K^{\downarrow\uparrow, \uparrow\downarrow}$  excitons. Our work provides microscopic insights into experimentally observed photoluminescence

spectra in presence of magnetic fields and overall sheds light on the excitonic landscape in 2D materials.

**Acknowledgments:** This project has received funding from the Swedish Research Council (VR, project number 2018-00734) and the European Union’s Horizon 2020 research and innovation program under grant agreement No 881603 (Graphene Flagship). Furthermore, we acknowledge support by the Chalmers Area of Advance in Nanoscience and Nanotechnology.

- <sup>1</sup> G. Wang, A. Chernikov, M. M. Glazov, T. F. Heinz, X. Marie, T. Amand, and B. Urbaszek, *Rev. Mod. Phys.* **90**, 021001 (2018).
- <sup>2</sup> T. Mueller and E. Malic, *npj 2D Materials and Applications* **2**, 1 (2018).
- <sup>3</sup> P. Merkl, F. Mooshammer, P. Steinleitner, A. Girnghuber, K.-Q. Lin, P. Nagler, J. Holler, C. Schüller, J. M. Lupton, T. Korn, *et al.*, *Nature materials* **18**, 691 (2019).
- <sup>4</sup> K. F. Mak, C. Lee, J. Hone, J. Shan, and T. F. Heinz, *Phys. Rev. Lett.* **105**, 136805 (2010).
- <sup>5</sup> G. Berghäuser and E. Malic, *Phys. Rev. B* **89**, 125309 (2014).
- <sup>6</sup> M. Selig, G. Berghäuser, A. Raja, P. Nagler, C. Schüller, T. F. Heinz, T. Korn, A. Chernikov, E. Malic, and A. Knorr, *Nature communications* **7**, 13279 (2016).
- <sup>7</sup> A. Kormányos, G. Burkard, M. Gmitra, J. Fabian, V. Zolyomi, N. D. Drummond, and V. Falko, *2D Materials* **2**, 022001 (2015).
- <sup>8</sup> H. Yu, M. Laurien, Z. Hu, and O. Rubel, *Physical Review B* **100**, 125413 (2019).
- <sup>9</sup> A. Chernikov, T. C. Berkelbach, H. M. Hill, A. Rigosi, Y. Li, O. B. Aslan, D. R. Reichman, M. S. Hybertsen, and T. F. Heinz, *Phys. Rev. Lett.* **113**, 076802 (2014).
- <sup>10</sup> A. Arora, M. Koperski, K. Nogajewski, J. Marcus, C. Faugeras, and M. Potemski, *Nanoscale* **7**, 10421 (2015).
- <sup>11</sup> M. Feierabend, G. Berghäuser, A. Knorr, and E. Malic, *Nature Communications* **8**, 14776 (2017).
- <sup>12</sup> M. Molas, C. Faugeras, A. Slobodeniuk, K. Nogajewski, M. Bartos, D. Basko, and M. Potemski, *2D Materials* **4**, 021003 (2017).
- <sup>13</sup> Z. Li, T. Wang, C. Jin, Z. Lu, Z. Lian, Y. Meng, M. Blei, S. Gao, T. Taniguchi, K. Watanabe, *et al.*, *Nature communications* **10**, 2469 (2019).
- <sup>14</sup> M. Selig, G. Berghäuser, M. Richter, R. Bratschitsch, A. Knorr, and E. Malic, *2D Materials* **5**, 035017 (2018).
- <sup>15</sup> E. Malic, M. Selig, M. Feierabend, S. Brem, D. Christiansen, F. Wendler, A. Knorr, and G. Berghäuser, *Physical Review Materials* **2**, 014002 (2018).
- <sup>16</sup> T. Deilmann and K. S. Thygesen, *2D Materials* **6**, 035003 (2019).
- <sup>17</sup> X.-X. Zhang, T. Cao, Z. Lu, Y.-C. Lin, F. Zhang, Y. Wang, Z. Li, J. C. Hone, J. A. Robinson, D. Smirnov, *et al.*, *Nature nanotechnology* **12**, 883 (2017).
- <sup>18</sup> X.-X. Zhang, Y. You, S. Y. F. Zhao, and T. F. Heinz, *Physical review letters* **115**, 257403 (2015).
- <sup>19</sup> J. Lindlau, M. Selig, A. Neumann, L. Colombier, J. Förste, V. Funk, M. Förg, J. Kim, G. Berghäuser, T. Taniguchi, *et al.*, *Nature communications* **9**, 2586 (2018).
- <sup>20</sup> J. Lindlau, C. Robert, V. Funk, J. Förste, M. Förg, L. Colombier, A. Neumann, E. Courtade, S. Shree, T. Taniguchi, *et al.*, *arXiv preprint arXiv:1710.00988* (2017).
- <sup>21</sup> Y. Zhou, G. Scuri, D. S. Wild, A. A. High, A. Dibos, L. A. Jauregui, C. Shu, K. De Greve, K. Pistunova, A. Y. Joe, *et al.*, *Nature nanotechnology* **12**, 856 (2017).
- <sup>22</sup> M. Feierabend, G. Berghäuser, M. Selig, S. Brem, T. Shegai, S. Eigler, and E. Malic, *Physical Review Materials* **2**, 014004 (2018).
- <sup>23</sup> S. Brem, A. Ekman, D. Christiansen, F. Katsch, M. Selig, C. Robert, X. Marie, B. Urbaszek, A. Knorr, and E. Malic, *Nano Letters* **20**, 2849 (2020).
- <sup>24</sup> C. Robert, T. Amand, F. Cadiz, D. Lagarde, E. Courtade, M. Manca, T. Taniguchi, K. Watanabe, B. Urbaszek, and X. Marie, *Physical Review B* **96**, 155423 (2017).
- <sup>25</sup> G. Wang, C. Robert, M. Glazov, F. Cadiz, E. Courtade, T. Amand, D. Lagarde, T. Taniguchi, K. Watanabe, B. Urbaszek, *et al.*, *Physical review letters* **119**, 047401 (2017).
- <sup>26</sup> R. Vasconcelos, H. Bragança, F. Qu, and J. Fu, *Physical Review B* **98**, 195302 (2018).
- <sup>27</sup> G.-H. Peng, P.-Y. Lo, W.-H. Li, Y.-C. Huang, Y.-H. Chen, C.-H. Lee, C.-K. Yang, and S.-J. Cheng, *Nano letters* **19**, 2299 (2019).
- <sup>28</sup> M. Baranowski, A. Surrente, D. Maude, M. Ballottin, A. Mitioglu, P. Christianen, Y. Kung, D. Dumcenco, A. Kis, and P. Plochocka, *2D Materials* **4**, 025016 (2017).
- <sup>29</sup> H. Haug and S. W. Koch, *Quantum Theory of the Optical and Electronic Properties of Semiconductors* (5th ed. (World Scientific Publishing Co. Pre. Ltd., Singapore, 2004).).
- <sup>30</sup> M. Kira and S. Koch, *Progress in Quantum Electronics* **30**, 155 (2006).
- <sup>31</sup> E. Malic and A. Knorr, *Graphene and Carbon Nanotubes: Ultrafast Optics and Relaxation Dynamics* (John Wiley & Sons, 2013).
- <sup>32</sup> F. Kadi, T. Winzer, E. Malic, A. Knorr, F. Göttfert, M. Mittendorff, S. Winnerl, and M. Helm, *Phys. Rev. Lett.* **113**, 035502 (2014).
- <sup>33</sup> A. Thränhardt, S. Kuckenburg, A. Knorr, T. Meier, and S. Koch, *Physical Review B* **62**, 2706 (2000).
- <sup>34</sup> A. Raja, L. Waldecker, J. Zipfel, Y. Cho, S. Brem, J. D. Ziegler, M. Kulig, T. Taniguchi, K. Watanabe, E. Malic, *et al.*, *Nature nanotechnology* **14**, 832 (2019).
- <sup>35</sup> F. Katsch, M. Selig, A. Carmele, and A. Knorr, *physica status solidi (b)* **255**, 1800185 (2018).
- <sup>36</sup> S. Brem, M. Selig, G. Berghäuser, and E. Malic, *Scientific reports* **8**, 8238 (2018).
- <sup>37</sup> J. Förste, N. V. Tepliakov, S. Y. Kruchinin, J. Lindlau, V. Funk, M. Förg, K. Watanabe, T. Taniguchi, A. S. Baimuratov, and A. Högele, *arXiv preprint arXiv:2002.11646* (2020).
- <sup>38</sup> G. Wang, L. Bouet, M. Glazov, T. Amand, E. Ivchenko, E. Palteau, X. Marie, and B. Urbaszek, *2D Materials* **2**, 034002 (2015).
- <sup>39</sup> A. Mitioglu, P. Plochocka, Á. Granados del Aguila, P. Christianen, G. Deligeorgis, S. Anghel, L. Kulyuk, and D. Maude, *Nano letters* **15**, 4387 (2015).
- <sup>40</sup> M. Koperski, M. R. Molas, A. Arora, K. Nogajewski, M. Bartos, J. Wyzula, D. Vaclavkova, P. Kossacki, and M. Potemski, *2D Materials* **6**, 015001 (2018).
- <sup>41</sup> V. Axt, K. Victor, and A. Stahl, *Physical Review B* **53**, 7244

- (1996).
- <sup>42</sup> Z. Khatibi, M. Feierabend, M. Selig, S. Brem, C. Linderälv, P. Erhart, and E. Malic, *2D Materials* **6**, 015015 (2018).
- <sup>43</sup> Z. Lu, D. Rhodes, Z. Li, D. Van Tuan, Y. Jiang, J. Ludwig, Z. Jiang, Z. Lian, S.-F. Shi, J. Hone, *et al.*, *2D Materials* **7**, 015017 (2019).
- <sup>44</sup> C. Robert, B. Han, P. Kapuscinski, A. Delhomme, C. Faugeras, T. Amand, M. Molas, M. Bartos, K. Watanabe, T. Taniguchi, *et al.*, arXiv preprint arXiv:2002.03877 (2020).
- <sup>45</sup> Z. Jin, X. Li, J. T. Mullen, and K. W. Kim, *Physical Review B* **90**, 045422 (2014).
- <sup>46</sup> K. Kaasbjerg, K. S. Thygesen, and K. W. Jacobsen, *Physical Review B* **85**, 115317 (2012).
- <sup>47</sup> M. Selig, F. Katsch, S. Brem, G. F. Mkrtchian, E. Malic, and A. Knorr, arXiv preprint arXiv:1908.11178 (2019).